Electronic supplementary information

for

A Photoconductive Charge-Transfer Crystal with Mixed-Stacking Donor-Acceptor Heterojunctions within Lattice

Wei Yu,[a,‡] Xiao-Ye Wang,[b,‡] Jing Li,[a] Zhi-Ting Li,[a] Yu-Kun Yan,[a] Wei Wang,[*,a] and Jian Pei[*,b]

[a] Center for Synthetic Soft Materials, Key Laboratory of Functional Polymer Materials of the Ministry of Education, Institute of Polymer Chemistry, Nankai University, Tianjin 300071, China.

[b] Beijing National Laboratory for Molecular Science (BNLMS), the Key Laboratory of Bioorganic Chemistry and Molecular Engineering, College of Chemistry and Molecular Engineering, Peking University, Beijing 100871, China.

‡Equivalent contribution

*Corresponding Author Email Addresses: weiwang@nankai.edu.cn and jianpei@pku.edu.cn

Outline of Figures:

Materials

1,3,6,8-pyrenetetrasulfonic acid tetrasodium salt hydrate (PyTs ≥98% HPLC) was purchased from Aldrich Chemical Co., 4,4'-Dipyridyl (99%) was purchased from J&K Chemical Co., and 1-bromobutane (99%) purchased from Fluka Chemie. All chemicals and solvents were used directly without any further purification and water was used after filtering by Millipore (resistivity>18.2 MΩ cm).

General methods

^{1}H NMR spectra were recorded in D_2O on a Varian Unity Plus-400 NMR spectrometer. 2D NOESY spectra were recorded on a Varian Mercury VX300 instrument.

UV–vis absorption spectra were recorded on a Hitachi U-3900H spectrophotometer using a quartz cell with a path length of 10mm. UV–vis spectra in solid state were recorded using a Shimadzu integrating sphere assembly attached to a Shimadzu UV-3600 spectrophotometer. $BaSO_4$ was used as the reflectance standard.

Fluorescence spectra were obtained with a Hitachi F-7000 spectrometer using a quartz cell with a path length of 10 mm. ESI-MS spectrometric analyses were performed on a Thermo Finnigan LCQ AD System.

Cyclic voltammetry (CV) experiments were performed with an LK98B II microcomputer-based electrochemical analyzer. All

measurements were carried out at room temperature with a conventional three-electrode configuration employing a glassy carbon electrode as the working electrode, a saturated calomel electrode (SCE) as the reference electrode, and a Pt wire as the counter electrode. CH_3CN was distilled over calcium hydride under dry argon immediately prior to use. Tetrabutylammonium hexafluorophosphate (Bu_4NPF_6, 0.1 M) in CH_3CN was used as the supporting electrolyte, and the scan rate was 20 mV s^{-1}.

Scanning electron microscopy (SEM) was carried out with a Shimadzu SS-550 operating at 15 kV.

X-ray Photoelectron Spectroscopy (XPS) spectra were recorded using a Kratos Axis Ultra DLD spectrometer employing a monochromated Al-Ka X-ray source ($h\nu$ = 1486.6 eV), hybrid (magnetic/electrostatic) optics and a multi-channel plate and delay line detector (DLD). XPS spectra were recorded using an aperture slot of 300 $\times$700 μm^2, survey spectra were recorded with a pass energy of 160 eV, and high resolution spectra with a pass energy of 40 eV.

Polarized optical microscopy (POM) experiments were performed using a BX51 Olympus optical microscope equipped with a digital camera.

Thermogravimetric (TG) analysis of CT crystal was measured by TG (NETZSCH, TG209) with a heating rate of 20 °C/min in nitrogen atmosphere.

Transmission electron microscopy (TEM) and selected area electron diffraction (SAED) patterns were performed with a JEOL 2100F field emission transmission electron microscope operated at 200 kV. Specimens for TEM and SAED measurements were prepared via carefully moving onto a copper grid, coated with an amorphous carbon supporting film of a conventional holey carbon microgrid.

X-ray structural determinations. Crystallographic data of the compound were collected on a Rigaku MM-07 Saturn 724 CCD diffractometer (Rigaku International Corp., Tokyo, Japan) using graphite-monochromated Mo Kα radiation (λ= 0.71073 Å) at 113(2)K. The structure was solved by direct methods (SHELXS-97)[S1] and refined by full-matrix least squares on F2. All non-hydrogen atoms were refined anisotropically and hydrogen atoms by a riding model (SHELXL-97)[S2].

Density functional theory (DFT) calculations were performed at the B3LYP level of theory with a 6-31G* basis set using the Gaussian 03 program.[S3]

Device Fabrication: The silicon wafer with 300 nm-thick SiO_2 was cleaned by sonication in acetone, detergent, pure water and isopropyl alcohol sequentially and was dried in a vacuum oven at 80 °C for 30 min. After treated with oxygen-plasma for 15 min, the substrate was spin-coated with a polystyrene (PS) solution in 1,2-dichlorobenzene and then was annealed at 80 °C for 30 min in the glovebox. The suspension of

microribbon was spin-coated onto the PS-coated substrates, which was dried overnight in a vacuum oven at 80 °C. A polyethylene (PE) fiber as the shadow mask was mounted on the substrate. Finally, a layer of silver with a thickness of 50 nm was deposited onto the ribbon by thermal evaporation under a pressure of 4×10^{-4} Pa with an improved plastic-fiber-mask method.

Photoconductive measurements: The single-crystal-based devices were measured in air using a Vector BX4000 probe station connected to a Keithley SCS 4200. The light irradiation was provided by a Coherent diode laser (CUBE 405c), with a wavelength of 405nm. The laser beam was directed to the sample through a glass optical fiber. The light power was measured by a photon detector. The light intensity was obtained by simply dividing the beam power by the spot size and was measured to be 100 mW/mm^2.

Synthetic route

1,1’-bibutyl-4,4’-bipyridinium dibromide (butyl-violegen, BuV) was obtained by a quaternization reaction of 4,4'-dipyridyl with 1-bromobutane.(Synthetic Details)

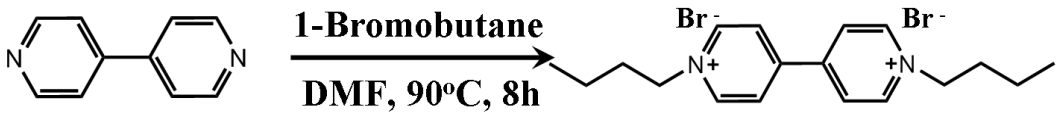

^{1}H NMR (400 MHz, D_2O, 298 K): δ 1.00 (t, 6H), 1.44 (t, 4H), 2.10 (t, 4H), 4.75 (t, 4H), 8.57(d, 4H), 9.15 (d, 4H).

Figure S1. Molecular orbital surfaces of the (a). Highest Occupied Molecular Orbital (HOMO) of PyTs, (b). HOMO-1 of PyTs, (c). Lowest Unoccupied Molecular Orbital (LUMO) of BuV.

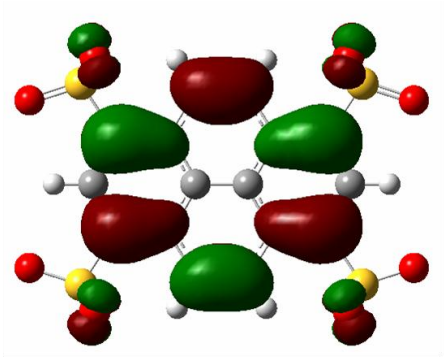

HOMO (PyTs) a

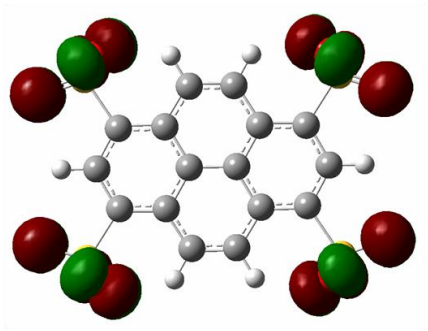

HOMO-1 (PyTs) b

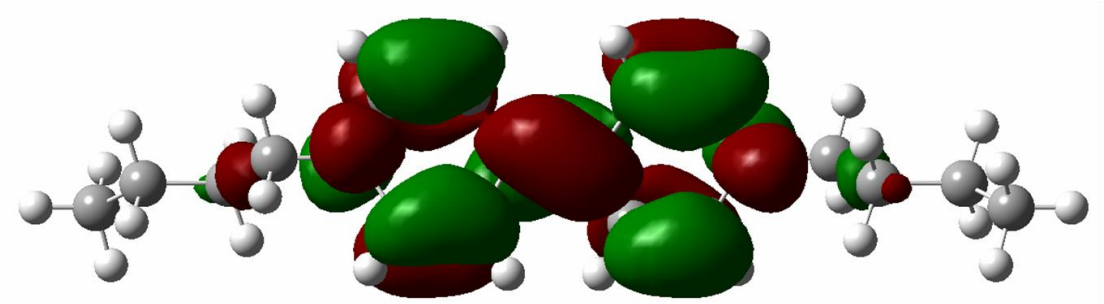

LUMO (BuV) c

Figure S2. ^{1}H NMR Spectra of PyTs, BuV and CT complex in D_2O (con. ca. 0.01M). The dot line shows the shift of the resonance signal.

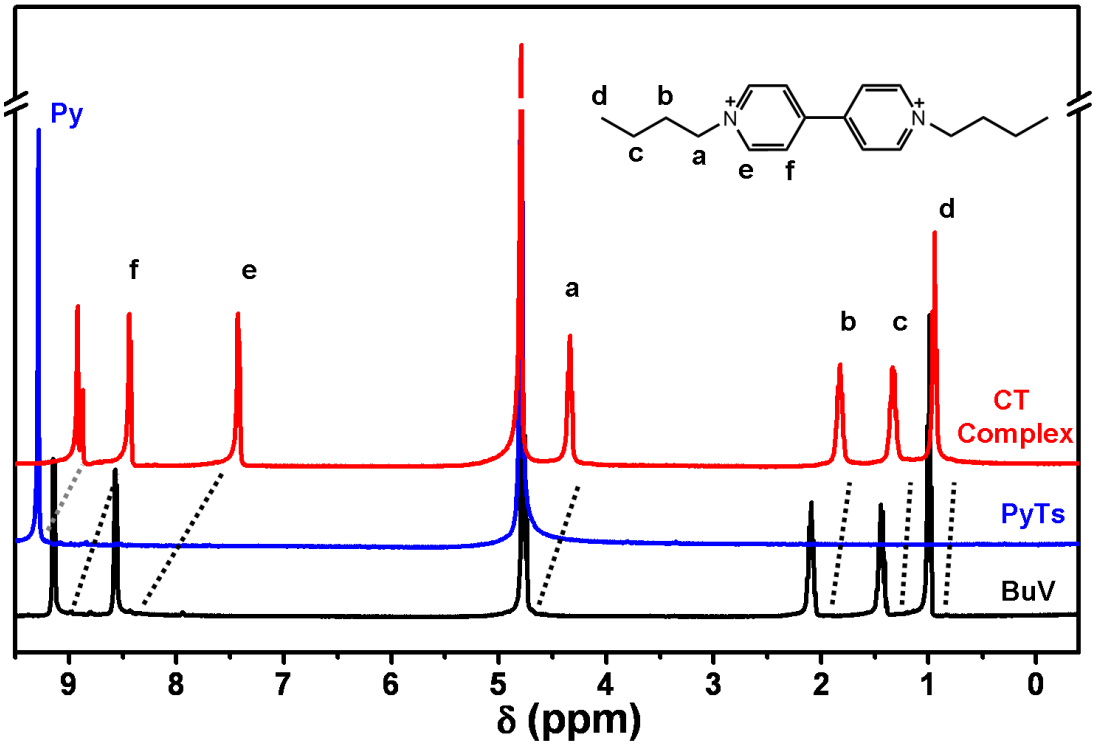

Figure S3. Photographs of PyTs, BuV and CT complex in water (con. ca. 0.01M), (a). under the normal light source (broad spectrum), (b). under the ultraviolet light (wavelength: 245nm).

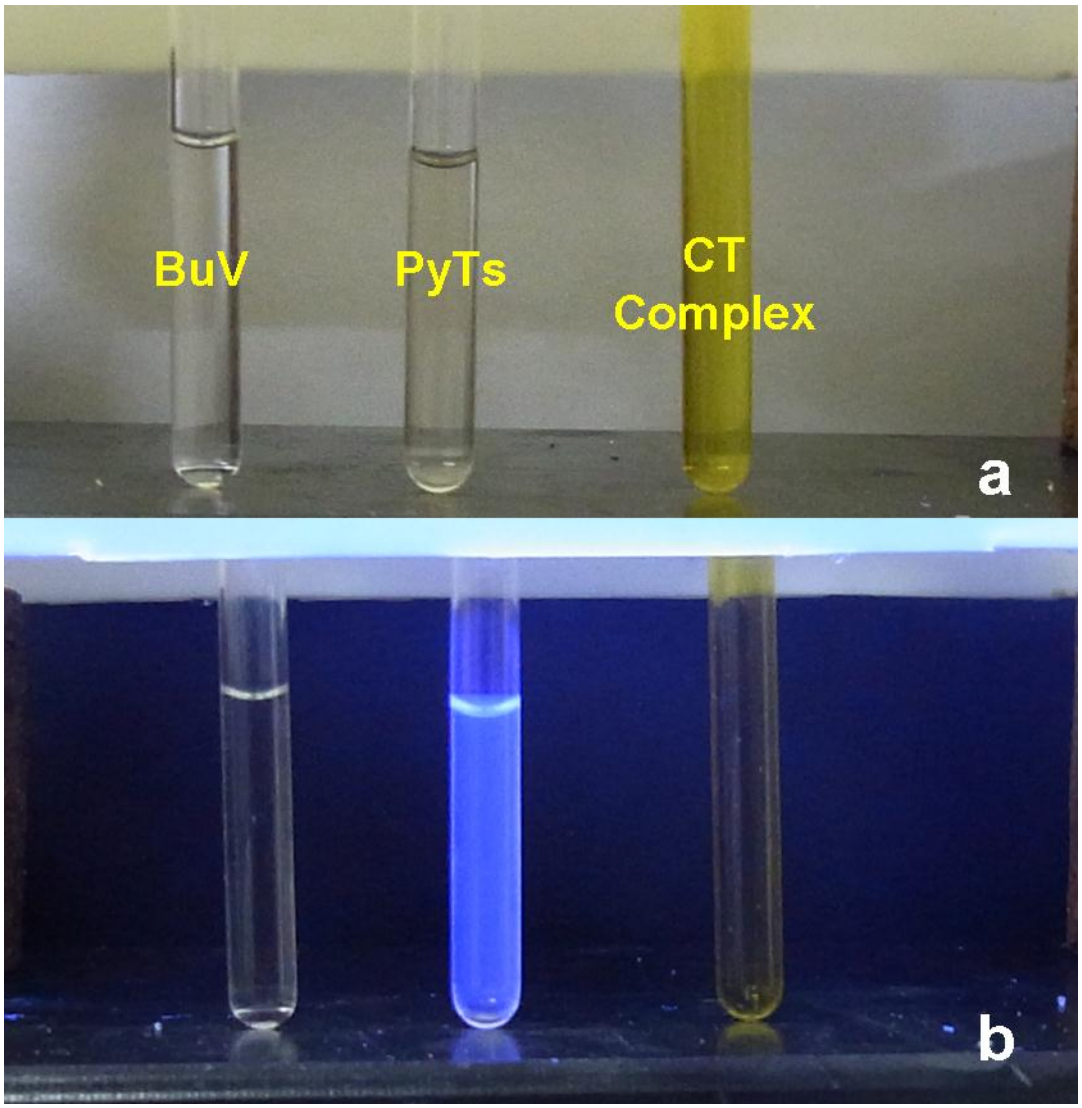

Figure S4. UV–vis absorption spectra (con. ca. 10^{-5} M).

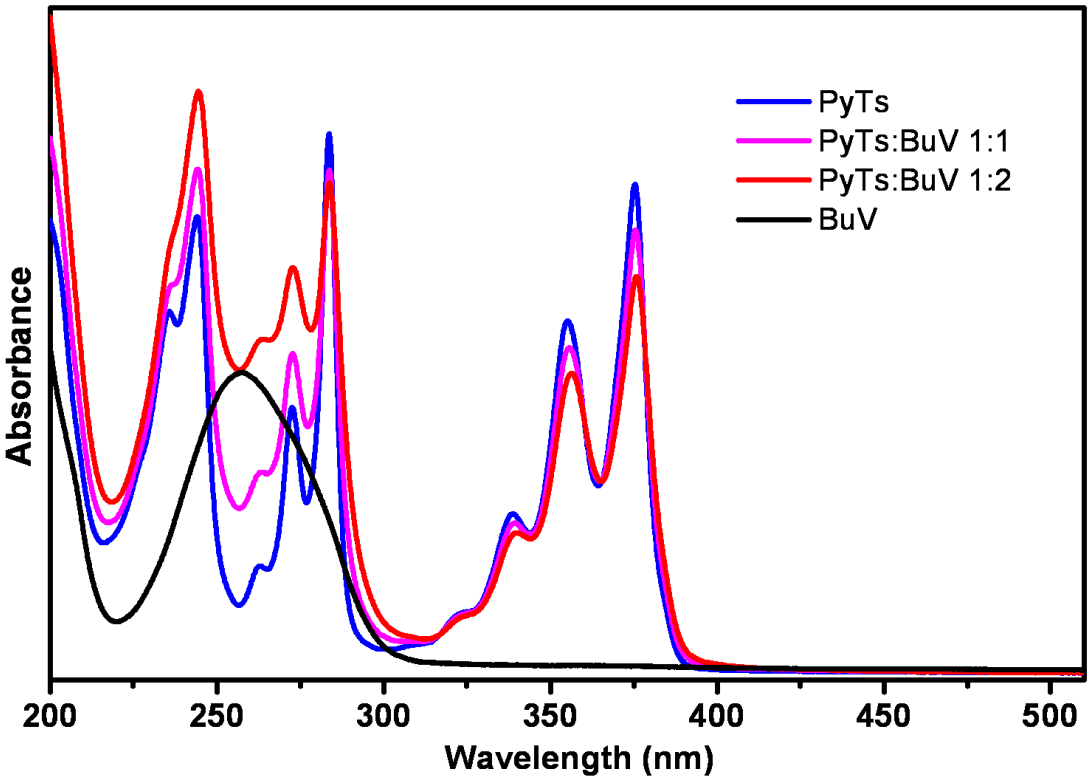

Figure S5. Stern-Volmer plot for the fluorescence quenching behavior of PyTs by BuV.

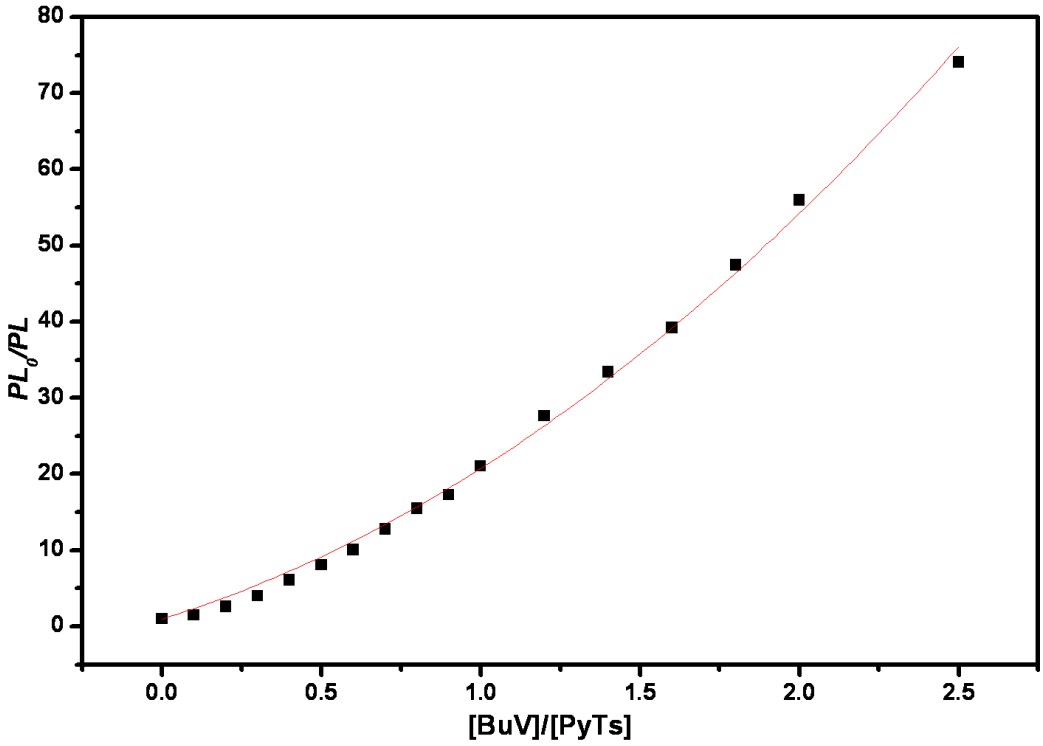

The fluorescence quenching behavior can be explained by the Stern-Volmer equation:

$$\frac{F_0}{F} = \tau/\tau_0 = 1 + K_{SV}[Q] \qquad \text{Eq.S1}$$

Where the F_0 is intensity of fluorescence in the absence of the quencher, F is the intensity of fluorescence in the presence of the quencher, τ and τ_0 is the corresponding fluorescence lifetime, [Q] is the concentration of the quencher, and K_{SV} is Stern-Volmer constant.

When the Sphere Of Action (SOA) is emerged, Eq.S1 can be written as:

$$\frac{F_0}{F} = (1 + K_D[Q])\exp([Q]VN/1000) \qquad \text{Eq.S2}$$

Where V is the volume of the SOA for one quencher molecule, N is Avogadro's constant.

When [Q]VN/1000 is much smaller than 1, Eq.S2 can be simplified as:

$$\frac{F_0}{F} = (1 + K_D[Q])(1 + [Q]VN/1000) \qquad \text{eq.S3}$$

That means the function [Q] vs F_0/F is a quadratic function, so the Stern-Volmer plot can be fitted with the function:

$y=1+12.88x+6.86x^2$

Figure S6. (a) ESI-MS spectrum of the CT complex. For the ESI-MS-MS, four typical spectra of the CT complex are given: (b)-(e) the numbers showed in the figure are the different percentages of the fully bombarding voltages used in the second stage of tandem MS.

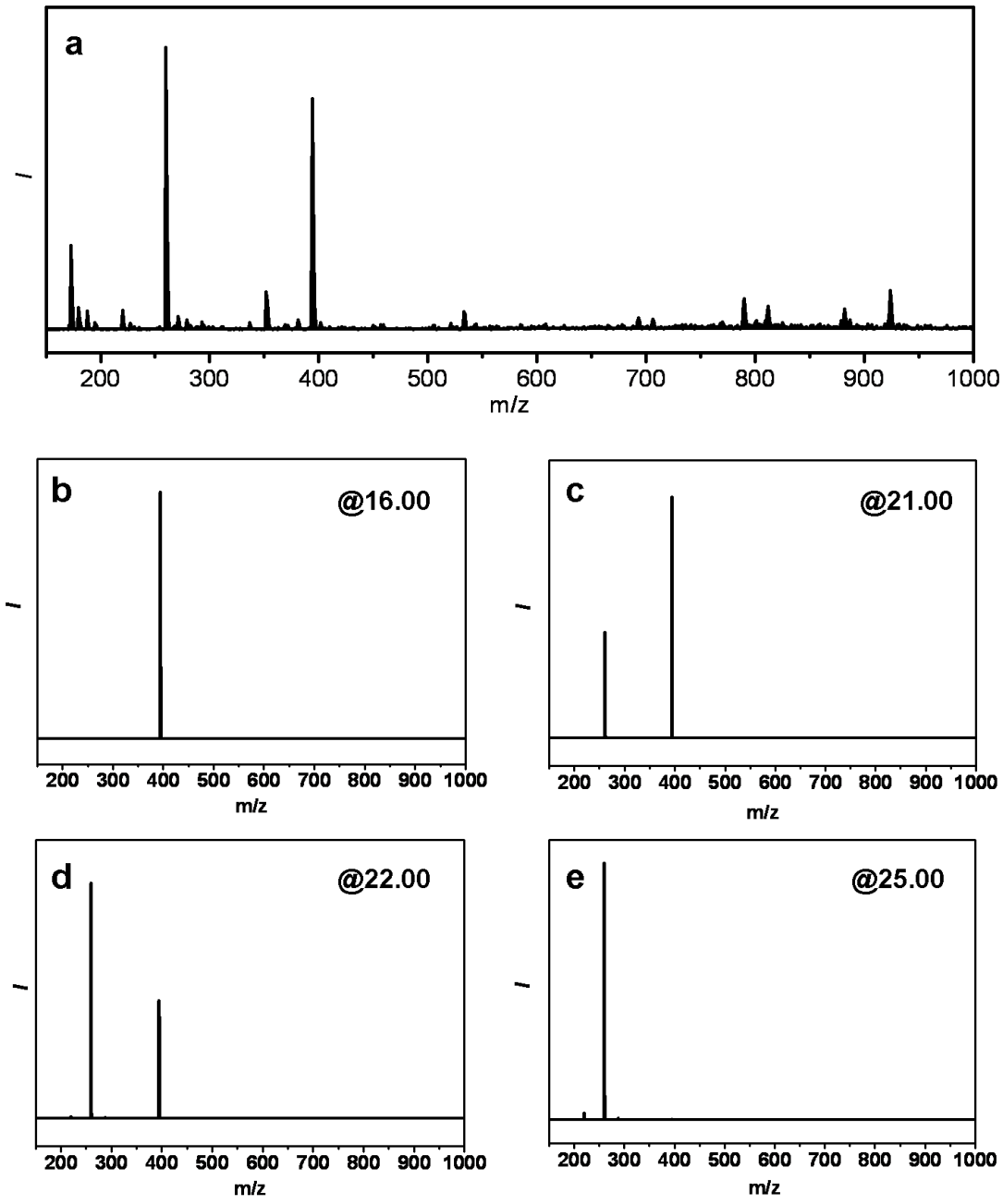

Figure S7. Current-voltage curves from cyclic voltammetry (CV) experiments (con. 0.2mM, red line: PyTs; blue line: BuV; black line: CT complex).

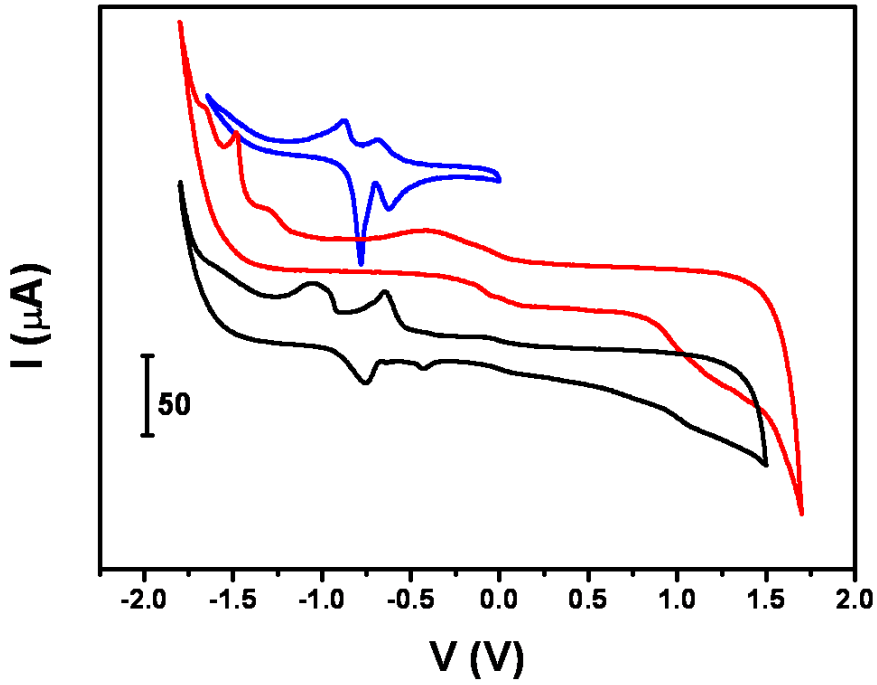

Table S1. Crystallographic parameters and the details of the structure refinements of the CT cocrystal.

Crystal data and structure refinement for CT crystal (BuV-PyTs)	
Empirical formula	$C_{52}H_{62}N_4O_{14}S_4$
Formula weight	1095.30
Temperature	113(2) K
Wavelength	0.71073 A
Crystal system, space group	Monoclinic, C2/c
Unit cell dimensions	a = 25.573(4) A
	b = 6.9899(10) A
	c = 28.737(5) A
	alpha = 90 deg.
	beta = 105.123(7) deg.
	gamma = 90 deg.
Volume	4958.8(14) A^3
Z, Calculated density	4, 1.467 Mg/m^3
Absorption coefficient	0.266 mm^{-1}
F(000)	2312
Crystal size	0.20 x 0.18 x 0.10 mm
Theta range for data collection	1.47 to 27.83 deg.
Limiting indices	-33<=h<=33, -8<=k<=9, -37<=l<=36
Reflections collected / unique	17353 / 5760 [R(int) = 0.0372]
Completeness to theta = 27.83	97.6 %
Absorption correction	Semi-empirical from equivalents
Max. and min. transmission	0.9739 and 0.9487
Refinement method	Full-matrix least-squares on F^2
Data / restraints / parameters	5760 / 3 / 344
Goodness-of-fit on F^2	1.025
Final R indices [I>2sigma(I)]	R1 = 0.0473, wR2 = 0.1306
R indices (all data)	R1 = 0.0664, wR2 = 0.1488
Largest diff. peak and hole	0.601 and -0.512 $e.A^{-3}$

Figure S8. Crystal structure of the CT cocrystal by stick mode (yellow: S, red: O, blue: N, dark gray: C, light gray: H).

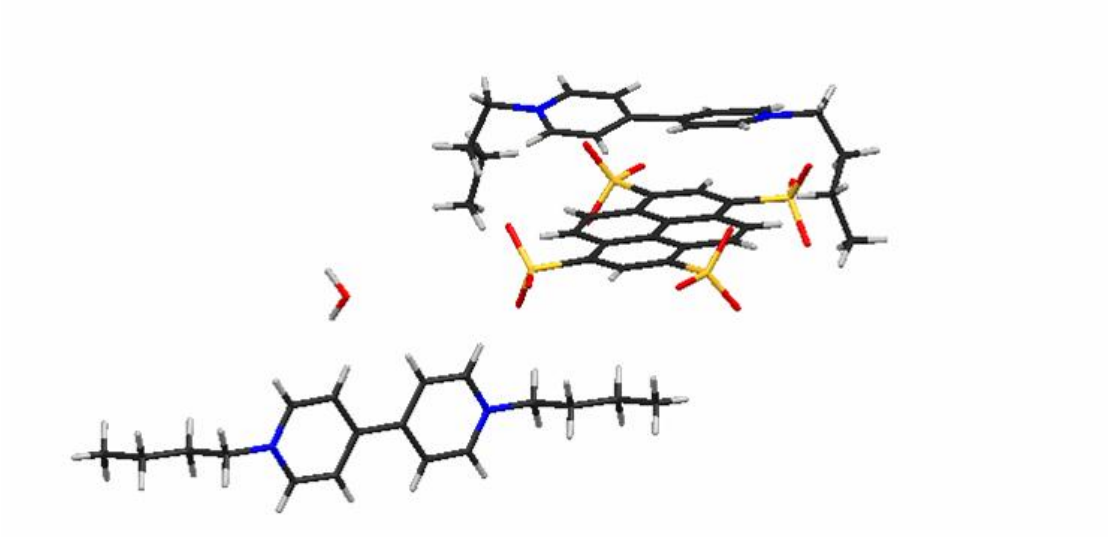

Figure S9. Crystal structure of the CT cocrystal and the details of the stacking volume.

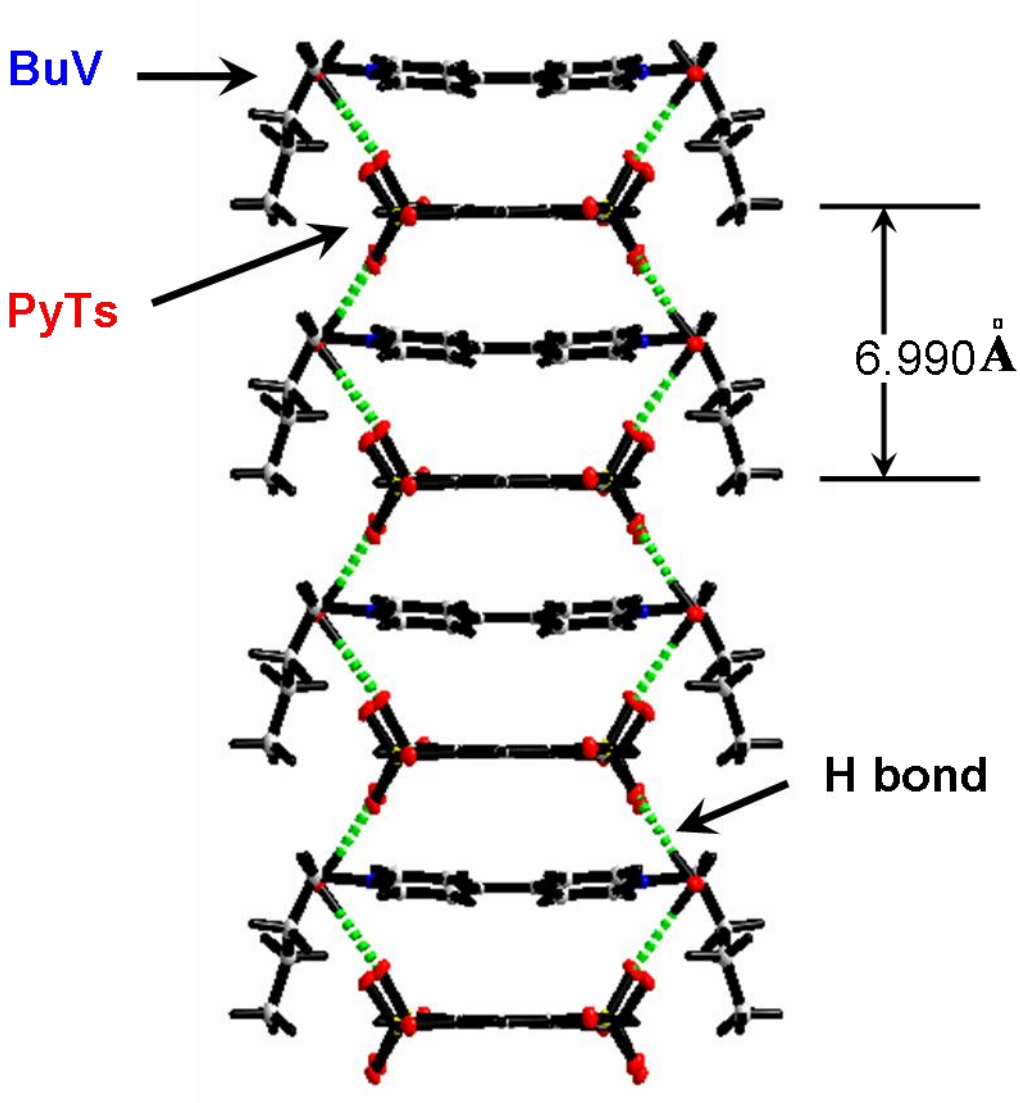

Figure S10. Photograph of the CT cocrystal as the large cyrstals.

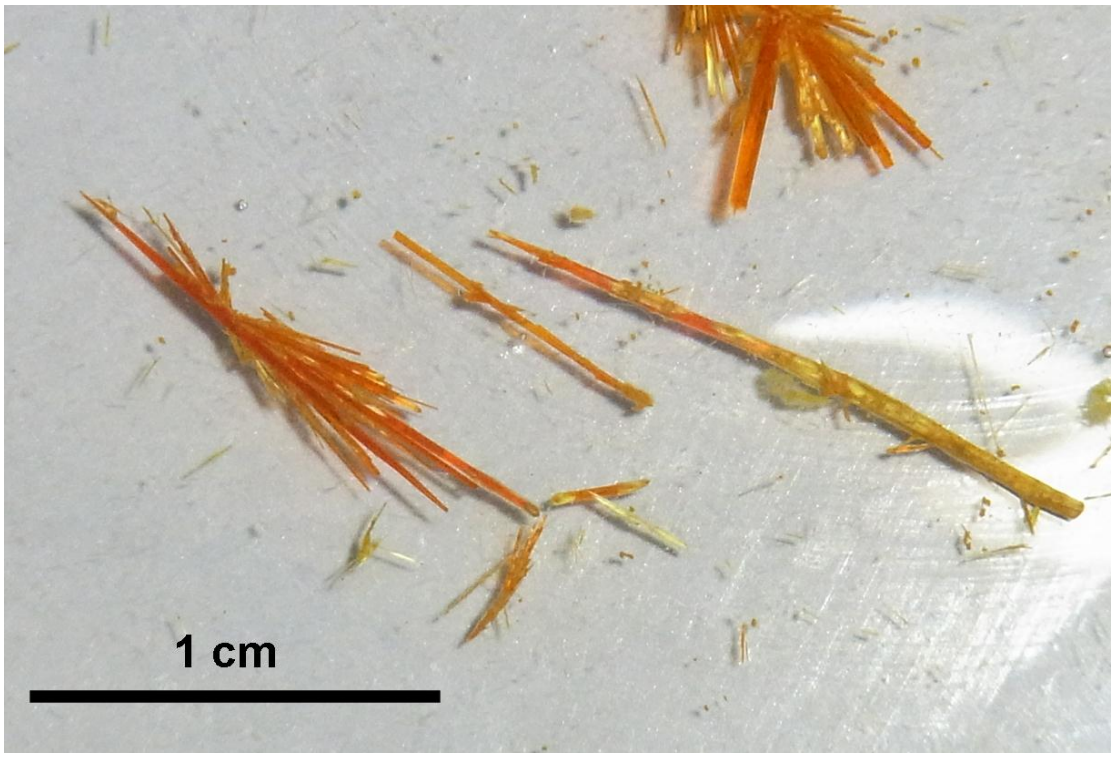

Figure S11. POM micrographs of the CT cocrystal.

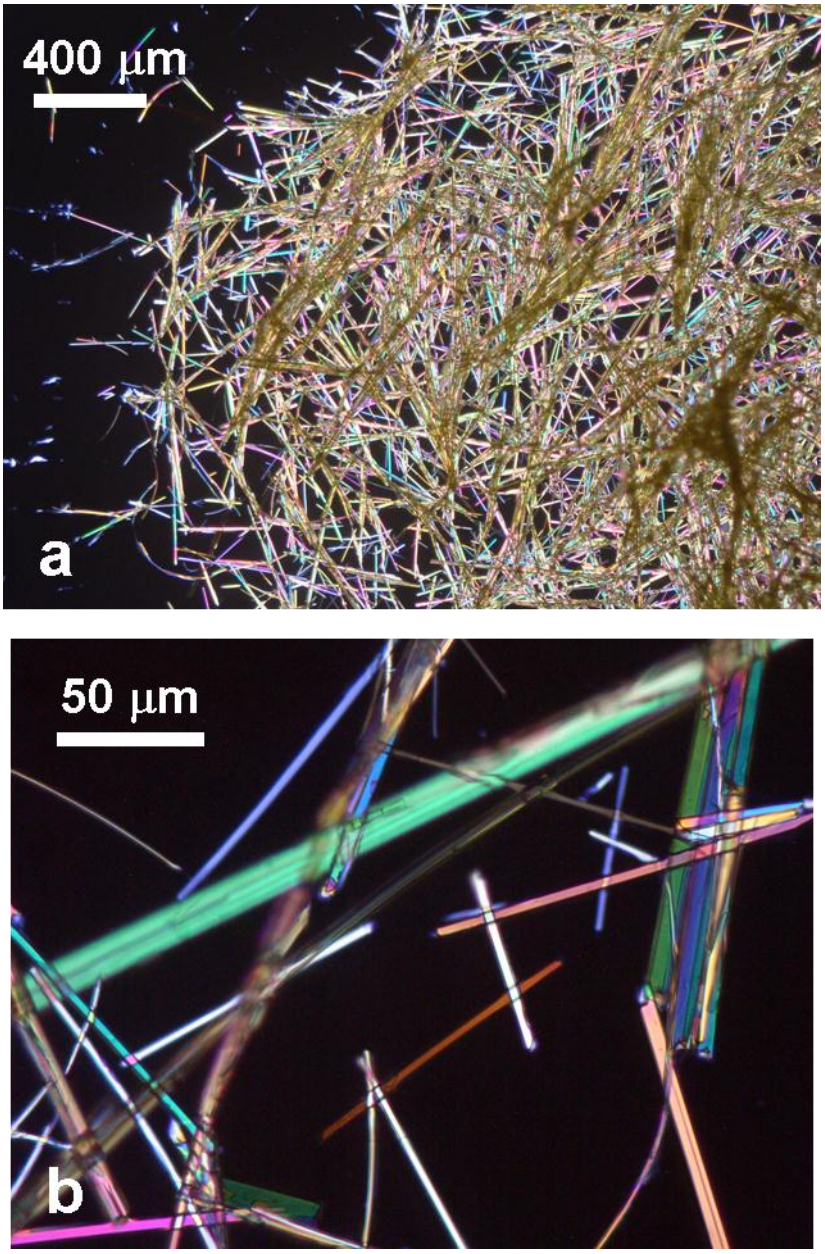

Figure S12. SEM micrographs of the CT cocrystal.

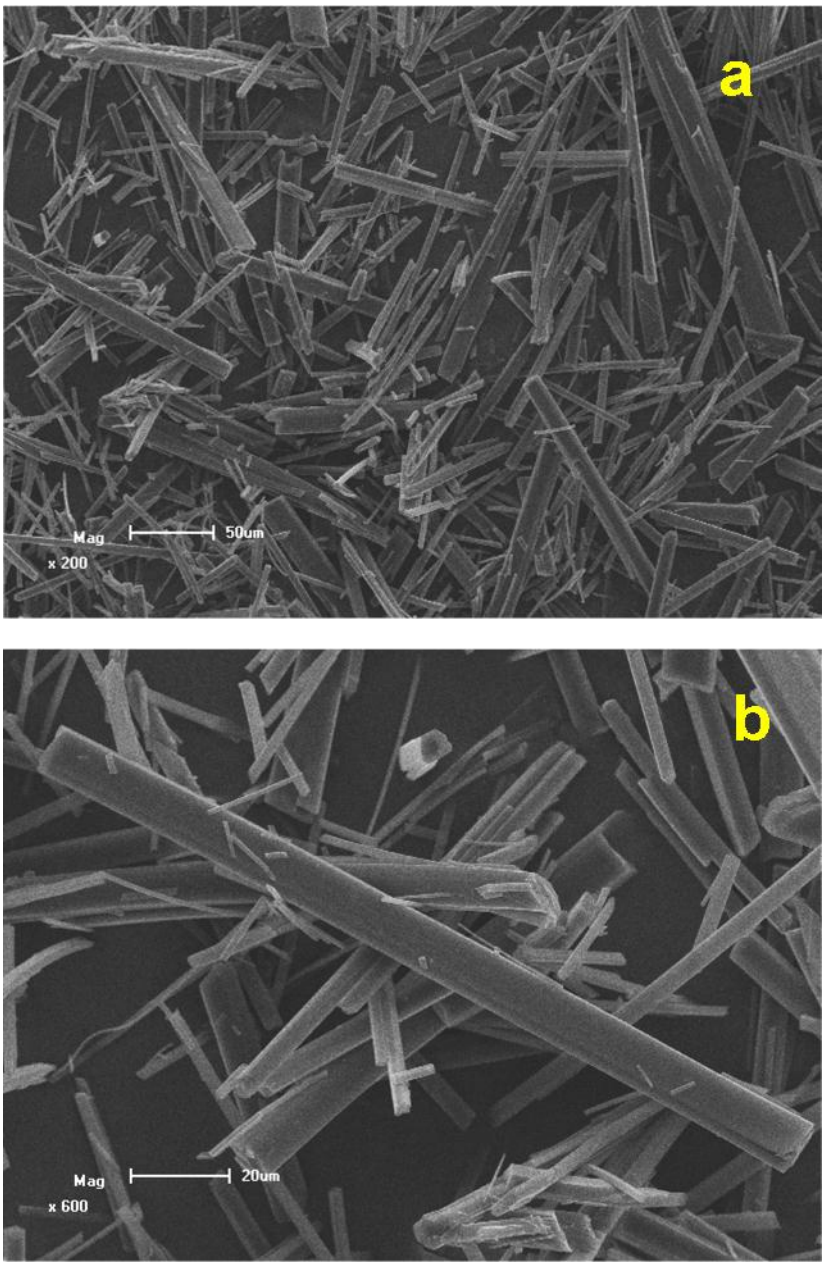

Figure S13. N 1s XPS spectra of (a). BuV, (b). CT cocrystals (solid line: experimental energy curves, dot line: assigning peak energy curves).

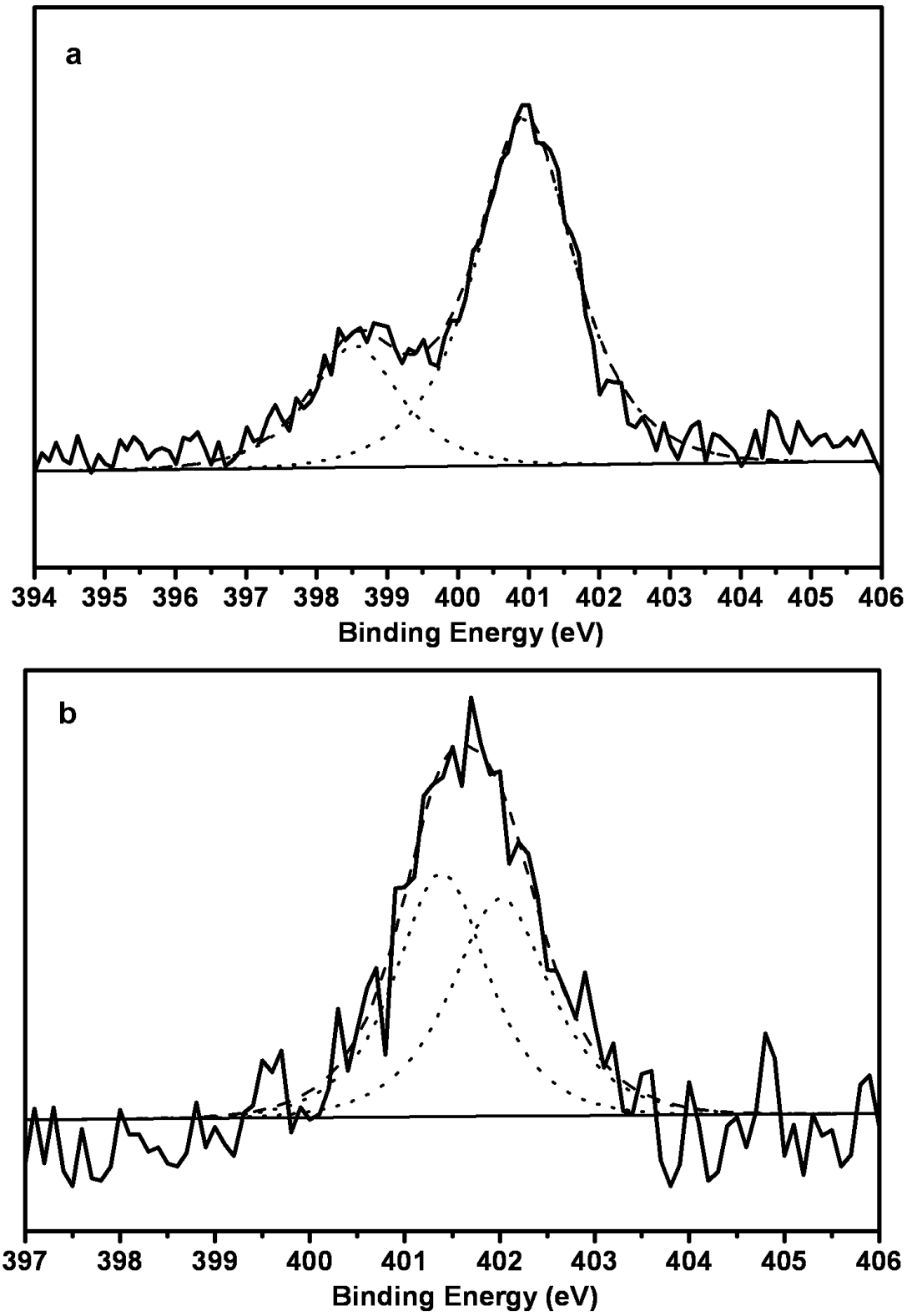

Figure S14. UV−vis absorption (diffuse reflectance) spectra. The absorption edges have been obtained by drawing tangent lines and show the numbers in the figure.

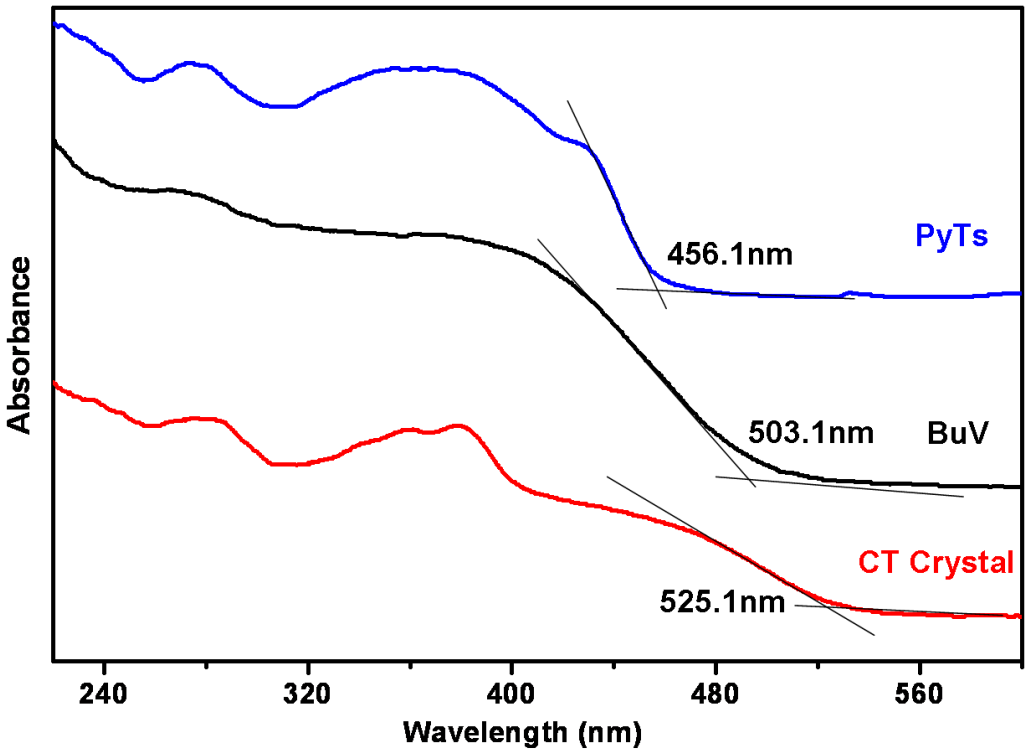

Figure S15. The original SAED patterns of the CT cocrystal. (The amplified part of Figure 3a (inset) in the article.)

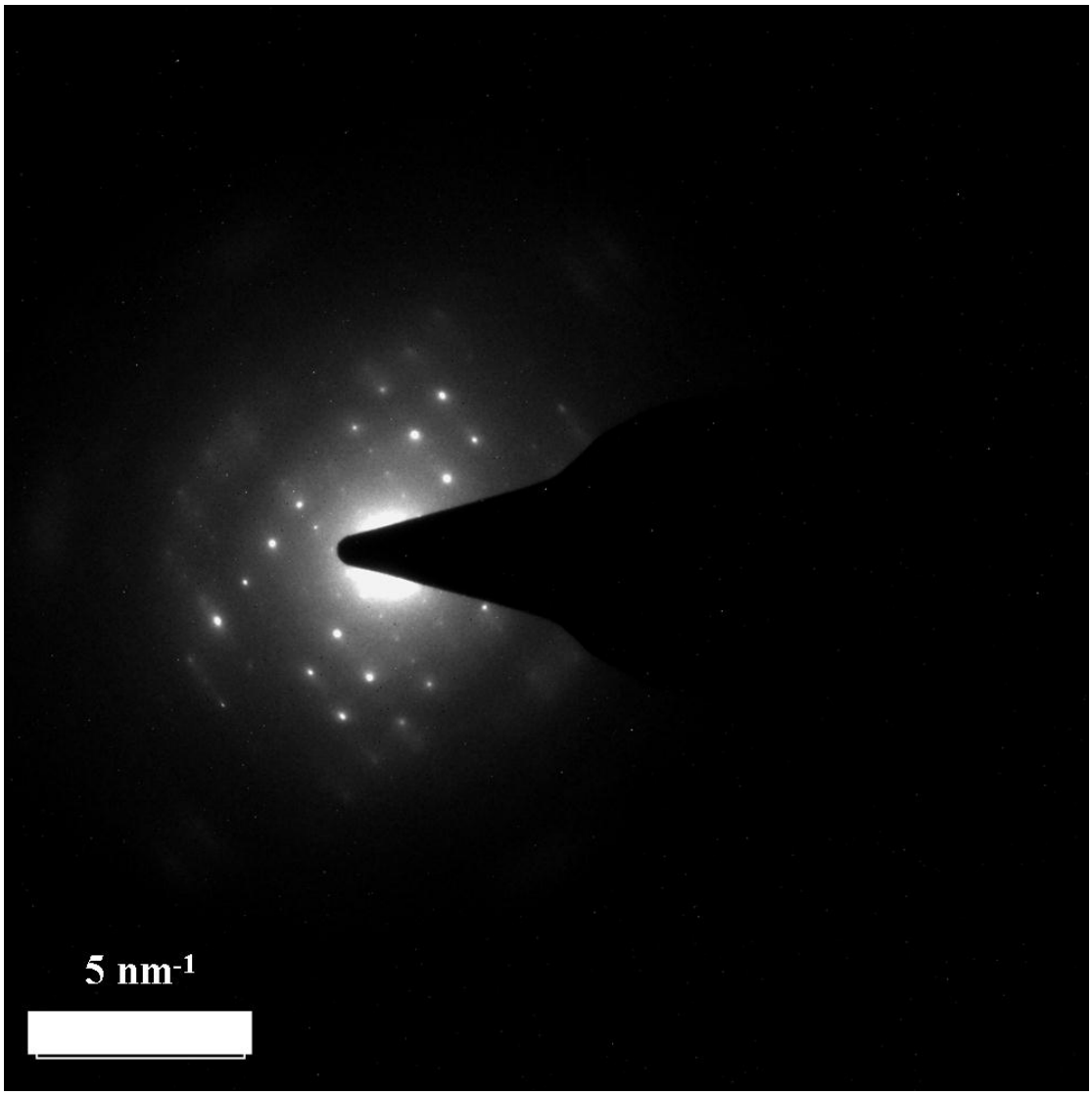

Figure S16. TG curve of the CT cocrystal.

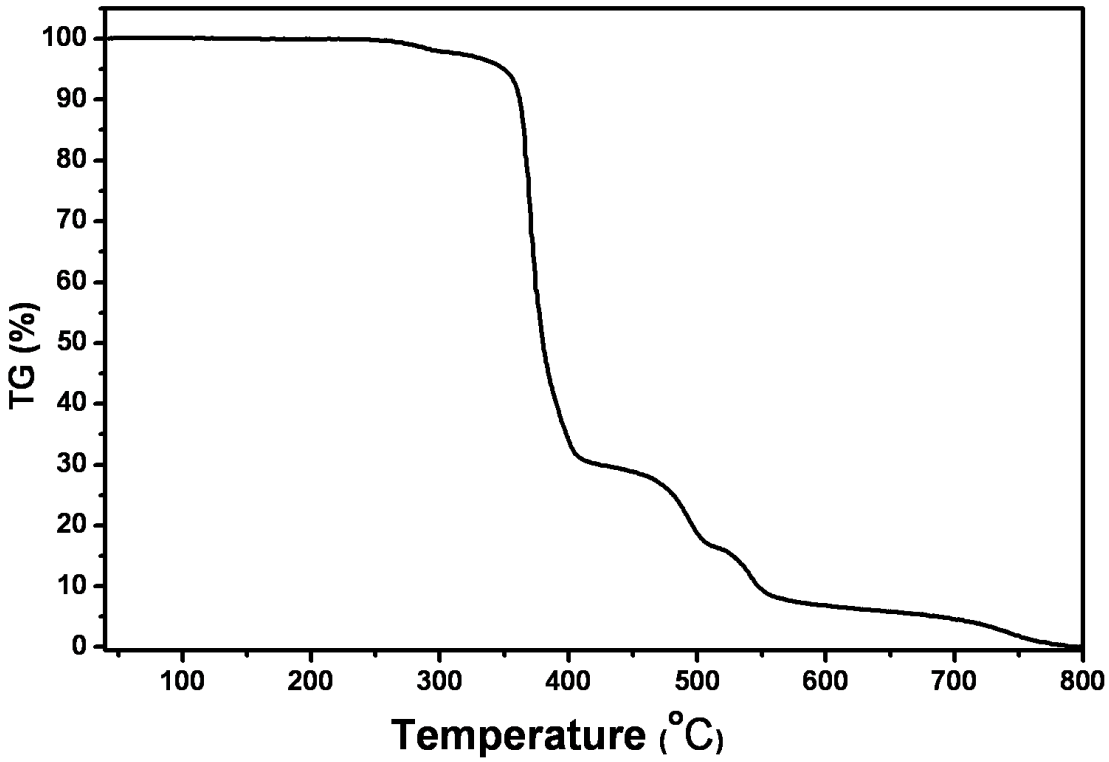

Density functional theory (DFT) calculations were friendly supported by Dr. Gao Peiyuan and Mr. Bai Zhiqiang, Beijing National Laboratory for Molecular Sciences, State Key Laboratory of Polymer Physics and Chemistry, Institute of Chemistry, Chinese Academy of Sciences, Beijing 100190, China.

Reference

S1 Sheldrick, G. M. SHELXS-90/96, Program for Structure Solution, Acta Crystallogr., Sect. A: Found. Crystallogr., 1990, 46, 467

S2 Sheldrick, G. M. SHELXL 97, Program for Crystal Structure Refinement, University of Goettingen, Goettingen, Germany, 1997

S3 Frisch, M. J.; Trucks, G. W.; Schlegel, H. B.; Scuseria, G. E.; Robb, M. A.; Cheeseman, J. R.; Montgomery, J. A., Jr.; Vreven, T.; Kudin, K. N.; Burant, J. C.; Millam, J. M.; Iyengar, S. S.; Tomasi, J.; Barone, V.; Mennucci, B.; Cossi, M.; Scalmani, G.; Rega, N.; Petersson, G. A.; Nakatsuji, H.; Hada, M.; Ehara, M.; Toyota, K.; Fukuda, R.; Hasegawa, J.; Ishida, M.; Nakajima, T.; Honda, Y.; Kitao, O.; Nakai, H.; Klene, M.; Li, X.; Knox, J. E.; Hratchian, H. P.; Cross, J. B.; Bakken, V.; Adamo, C.; Jaramillo, J.; Gomperts, R.; Stratmann, R. E.; Yazyev, O.; Austin, A. J.; Cammi, R.; Pomelli, C.; Ochterski, J. W.; Ayala, P. Y.; Morokuma, K.; Voth, G. A.; Salvador, P.; Dannenberg, J. J.; Zakrzewski, V. G.; Dapprich, S.; Daniels, A. D.; Strain, M. C.; Farkas, O.; Malick, D. K.; Rabuck, A. D.;

Raghavachari, K.; Foresman, J. B.; Ortiz, J. V.; Cui, Q.; Baboul, A. G.; Clifford, S.; Cioslowski, J.; Stefanov, B. B.; Liu, G.; Liashenko, A.; Piskorz, P.; Komaromi, I.; Martin, R. L.; Fox, D. J.; Keith, T.; Al-Laham, M. A.; Peng, C. Y.; Nanayakkara, A.; Challacombe, M.; Gill, P. M. W.; Johnson, B.; Chen, W.; Wong, M. W.; Gonzalez, C.; Pople, J. A. Gaussian 03, revision C.01; Gaussian, Inc.: Wallingford, CT, 2004.